Evidence of sudden rupture of a large asperity during the 2008 Mw7.9 Wenchuan earthquake based on strong motion analysis

Guohong Zhang,[1] Martin Vallée,[2] Xinjian Shan,[1] and Bertrand Delouis[2]

Received 1 June 2012; revised 30 July 2012; accepted 3 August 2012; published 13 September 2012.

[1] We investigate the rupture process of the 12 May 2008 Wenchuan earthquake using the records of 26 strong-motion stations, located 20–120 km from the seismic fault and with a good azimuthal coverage. The wave velocity model required to conduct this analysis has been validated against aftershocks, for which the point source hypothesis is a very good approximation. The inversion of the main shock rupture process confirms the slip distribution and the average rupture velocity (∼3 km/s) previously determined. However, a very peculiar behavior is clearly resolved by the extensive data set used in this study: the major slip area of the Wenchuan earthquake, located at 20–50 km North-East of the epicenter, is shown to break almost simultaneously, 25 s after earthquake initiation. This implies that slip in this part of the fault cannot be understood by simple stress release at the rupture front. A more likely interpretation is the presence of a strong asperity, which could break only when it was completely surrounded by stress increase, resulting in a delayed but brutal rupture. **Citation:** Zhang, G., M. Vallée, X. Shan, and B. Delouis (2012), Evidence of sudden rupture of a large asperity during the 2008 Mw7.9 Wenchuan earthquake based on strong motion analysis, *Geophys. Res. Lett.*, *39*, L17303, doi:10.1029/2012GL052516.

1. Introduction

[2] The May 12, 2008 Wenchuan earthquake was a predominantly thrusting event with some dextral slip, associated with over 240 km-long surface scarps along the Yingxiu-Beichuan Fault (YBF) and around 70 km-long scarps along the Guanxian-Jiangyou Fault (GJF), which is sub-parallel to YBF at its southwestern part [*Zhang et al.*, 2010]. The event occurred on the Long Men Shan Fault zone (LMSF), which is a northeast-southwest striking and northwest dipping fault zone separating the Tibetan plateau to the northwest from the Sichuan Basin to the southeast [*Burchfiel et al.*, 2008]. Previous rupture process studies have essentially used two types of datasets. On one hand, teleseismic data have been inverted to retrieve the main spatio-temporal features of the earthquake [e.g., *Ji and Hayes*, 2008; *Y. Zhang et al.*, 2009]. *Xu et al.* [2009] and *Zhang et al.* [2010] have also analyzed the teleseismic data using array analysis, in order to locate the high frequency source emission [*Krüger and Ohrnberger*, 2005; *Ishii et al.*, 2005]. However, due to the spatio-temporal integration effects of teleseismic data, it is difficult to gain knowledge about the complexity of the rupture process using only this data [e.g., *Menke*, 1985]. On the other hand, as the ALOS satellite has provided a wealth of SAR images with high coherence, the fault source model has also been estimated by inversion of InSAR measurements, which yet can only provide static slip distribution and bear no information on the temporal behavior of the earthquake [e.g., *Shen et al.*, 2009; *Feng et al.*, 2010]. As a general overview of the Wenchuan earthquake rupture process, we recall that teleseismic and geodetic data were able to resolve the average rupture velocity (3 km/s), the existence of two peak-slip areas around Yingxiu and Beichuan, and a strong increase of the strike-slip component in the northeastern part [e.g., *Zhang et al.*, 2010; *Shen et al.*, 2009]. Despite the comprehensiveness of the previous studies, it is still unclear how the rupture in the large slip areas has initiated and propagated. In this study, the spatial and temporal complexity of the rupture process of the Wenchuan earthquake is addressed by the analysis of the local strong motion data.

[3] The Wenchuan earthquake is the first of the major intra-continental earthquake (near Magnitude 8) to be covered by such a dense local network (Figure 1). In the past, only few and smaller scale events, like the 1992 Landers (California), 1999 Chichi (Taiwan) or the 2000 Tottori (Japan) earthquakes, were similarly recorded by a dense array of accelerometers. Compared to teleseismic data, local data presents the advantage of a strong sensitivity to the nearest points of the fault. Thus analysis of the latter dataset resolves out much greater detail of the rupture process along the seismic fault. To our best knowledge, the Wenchuan strong motion data have not been used yet in this respect, but only to determine the amplitude and duration of maximum shaking [*Li et al.*, 2008; *Wen et al.*, 2010]. Based on 26 stations located close to the fault (in the range 20–120 km), we describe here how the Wenchan rupture has developed over space and time, which in return will provide some evidence in order to discuss the classical dynamic rupture models, such as the asperity and barrier models [*Kanamori and Stewart*, 1978; *Das and Aki*, 1977].

2. Data, Fault Geometry and Inversion Scheme

[4] The National Strong-Motion Observation Network System (NSMONS) of China has begun operation about two months before the Wenchuan main shock. It has provided over 1,400 accelerogram components from the earthquake, belonging to 460 permanent strong motion stations distributed all over the country [*Li et al.*, 2008]. Taking into account the distance to the epicenter and the azimuth coverage of the rupture, we select 72 components from 26 stations to investigate the source faulting, among them 20 stations

[1]State Key Laboratory of Earthquake Dynamics, Institute of Geology, China Earthquake Administration, Beijing, China.
[2]GeoAzur, University of Nice Sophia-Antipolis, IRD, OCA, Valbonne, France.

Corresponding author: G. Zhang, State Key Laboratory of Earthquake Dynamics, Institute of Geology, China Earthquake Administration, Beijing 100029, China. (zhanggh@ies.ac.cn)

0094-8276/12/2012GL052516

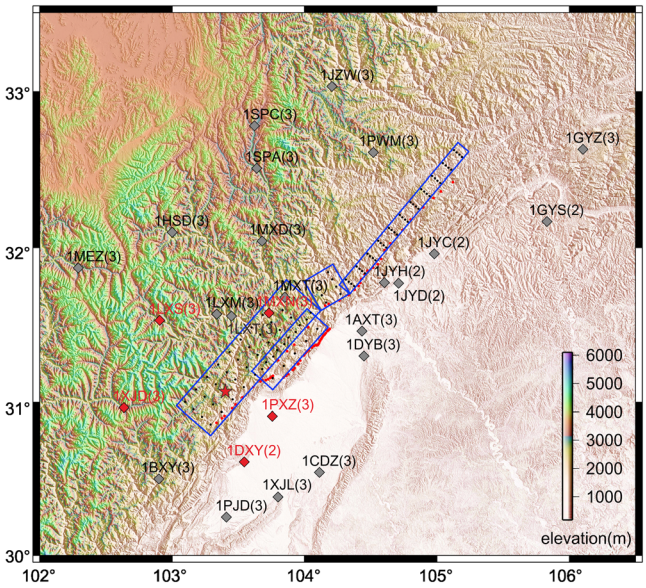

Figure 1. Distribution of the selected strong motion stations. The topography from SRTM3 is shown in the background. Blue rectangles and black points are the fault segments projected to the surface and the center of each subfault, respectively. Red points and red star are the fault surface ruptures determined from SAR image offset tracking and the epicenter location, respectively. The number of components available for each station is indicated after the station name (in parentheses). Stations marked with red are used to illustrate the differences between the optimal inversion and an inversion test in Figure 4.

with 3 components and 6 stations where only 2 components were available (Figure 1). All these stations are located between 20 km and 120 km from the ruptured fault and well distributed around it.

[5] In order to check our ability to model the waveforms, we first analyze two aftershocks (2008/05/13, 07h07 and 2008/05/25, 08h21) recorded by the strong motion stations. The main goal of this preliminary study is the determination of a suitable velocity model. As expected by the location of the fault between two different tectonic contexts (Sichuan Basin and Eastern Tibetan Plateau), the waveforms require two different models at NorthWest and SouthEast sides of the ruptured fault, respectively. The two main features of the velocity model are (1) a Moho depth of 50 km [*Xu and Song*, 2010; *Z. Zhang et al.*, 2009] and (2) the presence of a 4 km thick sedimentary layer in the Sichuan basin, to account for the upper Triassic layer [*Guo et al.*, 1996; *Meng et al.*, 2005]. We show in Texts S1 and S2 in the auxiliary material that a point-source modeling, using source parameters close to Global CMT (www.globalcmt.org) and the velocity models presented in Table 1, is able to reproduce the displacements generated by two aftershocks (magnitudes close to 6), for frequencies up to 0.1 Hz.

[6] We therefore use this velocity model and a high frequency cutoff of 0.1 Hz to model the main shock. The low-frequency cutoff of each component is determined by the original accelerogram noise level. Depending on the data quality, this cutoff varies between 0.008 Hz and 0.025 Hz.

[7] We establish a 4-segment fault model through matching the offsets of Synthetic Aperture Radar (SAR) satellite images (Figure 1) [*Zhang et al.*, 2011]. The main rupture of YBF is represented by 3 segments and the secondary rupture of GJF by 1 segment. The dip angles of YBF are varying from moderate (47°) on the southwest segment, to steeper (60°) on the middle, and even near vertical (78°) on the northeast segment, by integrating the results of our previous study of the InSAR data [*Zhang et al.*, 2011]. The dip angle of GJF is set to be 33°, so that the two fault segments converge to a shear zone at depth [*Zhang et al.*, 2010]. The rake is allowed to vary between 90° and 180°on each segment, to be consistent with thrust and dextral faulting. Each fault segment is discretized into subfaults measuring 12 km along strike and dip. The segments along the YBF have a fault width of 48 km (4 subfaults), consistent with the study of *Bjerrum et al.* [2010]. These authors have determined a fault width of 40 km, by comparing the slip inversion models with the hybrid ground motion simulation simulations. As we aim at a precise spatio-temporal determination of the earthquake process, the hypocentral location is important. We re-estimate the epicentral location by studying the initial polarization of the P waves recorded on the accelerograms (Text S3). To do so, we follow the general ideas presented by *Alessandrini et al.* [1994, and references therein] and *Scherbaum and Johnson* [1990]. Due to the excellent coverage of the stations, the back-azimuths deduced from the initial wave emissions converge to a small and well-defined area, very close to the location (31.06°N, 103.40°E). Using this epicentral location and the fault geometry, we locate the hypocentral depth at 13 km.

[8] Rupture process of an earthquake is often obtained based on the representation theorem of the slip source as a discontinuity in an elastic medium and a linear inversion solution for the discretization problem [*Olson and Aspel*, 1982]. Here in this study we use a multi-time window inversion scheme and simulated annealing algorithm to explore the model space, which allows for a multiple segment fault

[1]Auxiliary materials are available in the HTML. doi:10.1029/2012GL052516.

Table 1. Elastic Parameters of the Layered Crust Models

Station Type	Number of Layers	Depth / km	Vp (km/s)	Vs (km/s)	Rho (kg/m^3)
Stations within the Sichuan basin	1	0.0 – 4.0	4.0	2.3	2100.0
	2	4.0 – 50.0	6.0	3.4	2600.0
	3	∝	8.1	4.6	3400.0
Stations out of the Sichuan basin	1	0.0 – 50.0	6.0	3.4	2600.0
	2	∝	8.1	4.6	3400.0

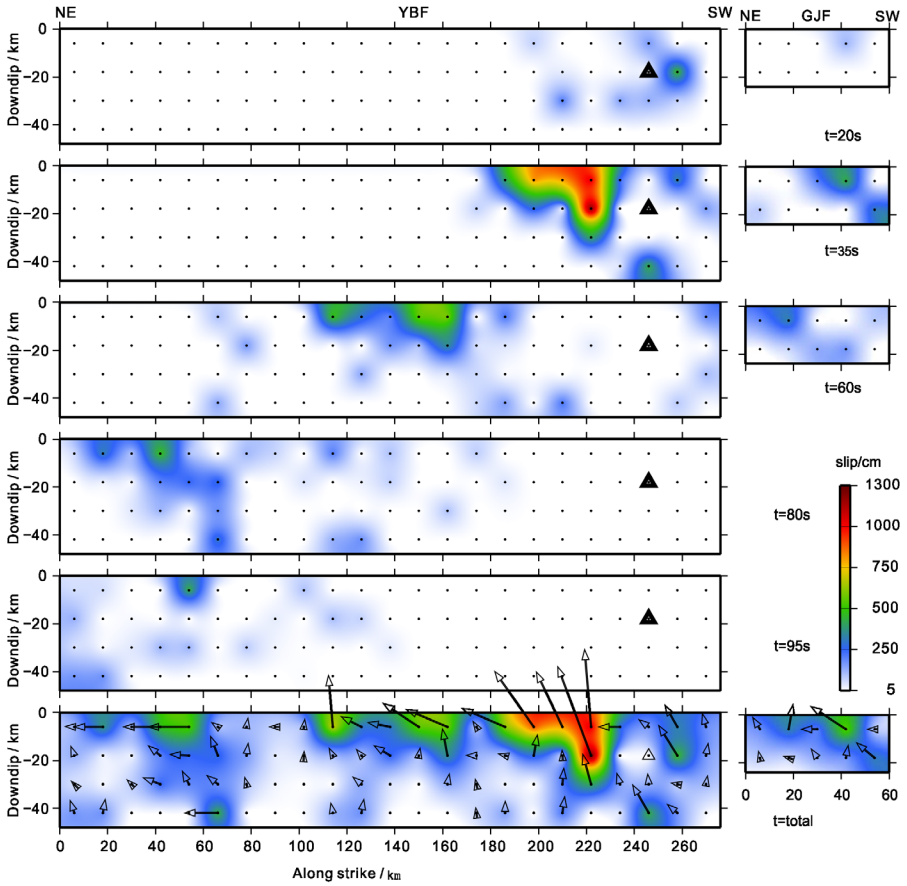

Figure 2. Snapshots of the rupture process of the Wenchuan earthquake. For clarity, the 3 segments of the YBF have been joint together. For the first 5 top panels, the time of each snapshot is shown on the right, and only the additional slip since the previous snapshot is presented. The last panel displays the final static slip and rake distribution (rake is shown only when slip is larger than 50 cm).

geometry, variable slip, and variable rupture velocity [*Delouis et al.*, 2002]. Convergence of the simulated annealing inversion is based on the simultaneous minimization of the normalized root mean square misfit of the strong motion waveforms and of the total seismic moment. We use three isocele triangular functions with 4 s half duration, mutually overlapping, to represent the individual source time function of each subfault. This allows a local duration up to 16 s, consistent with maximum expected slip (about 12 m) and typical slip rates (1 m/s). The onset times of each subfault are parameterized by the average rupture velocity from the hypocenter, which can vary from 1.0 to 3.8 km/s.

3. Inversion Results

[9] Figure 2 shows snapshots of the rupture process and the final static slip distribution of the Wenchuan earthquake. The overall fit of the strong motion data is good at most of the stations and the normalized rms misfit function is 0.42 (Figure S6). The slip distribution is dominated by a large slip patch located 20–50 km northeast from the epicenter. Three other moderate slip areas are also visible, at 90 km, 130 km, and 190 km northeast from the epicenter, respectively. The Wenchuan earthquake exhibits mainly reverse motion on the southwest segment. Motion tends to be more oblique (reverse-right lateral) in the middle segment, and purely right lateral in the northeast segment. Our final slip and rake distribution model is generally consistent with previously published models, especially those inverted from InSAR and GPS data [e.g., *Shen et al.*, 2009; *Feng et al.*, 2010; *Tong et al.*, 2010].

[10] Figure 3 allows to better figure out the spatio-temporal properties of the Wenchuan earthquake. It first shows that the unilateral rupture propagation along the LMSF lasted for about 90–95 s. While we have permitted a large variation for the rupture velocities (see the two thick lines corresponding to constant rupture velocity equal to 1.0 and 3.8 km/s), most radiating points of the middle and end of the fault are at the first order aligned with a 3 km/s constant rupture velocity. This is similar to the average rupture velocities determined by teleseismic data inversion or array analyses [*Wang et al.*, 2008; *Z. Zhang et al.*, 2009; *Xu et al.*, 2009; *Zhang and Ge*, 2010]. The high density of local strong motion data allows us to capture more details of the earthquake propagation, the most interesting one concerning the first 30 s of the rupture process. The earthquake initially ruptured bilaterally both to the northeast and southwest, but mainly to the northeast. While advancing in the northeast direction, it ruptured the contour of an irregular-shaped area, which will form latter on the main slip zone of the earthquake. This area which is located 20–50 km northeast of the hypocenter remains essentially unruptured

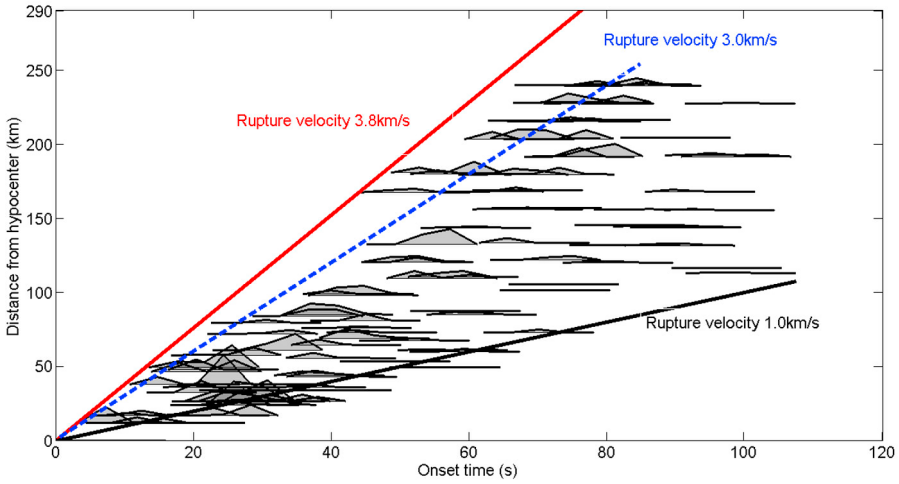

Figure 3. Time-distance plot of the moment release during the Wenchuan earthquake. The local source functions (STFs) of each point of the fault (parametrized by 3 overlapping triangles with a half-duration of 4 s) are shown on the figure. Each STF is located by its scalar distance to the hypocenter (vertical scale). On the horizontal scale, the STFs are shown with respect to the rupture initiation time. Their onset time was allowed to vary between the black and red curves (corresponding to average rupture velocity of 1 km/s and 3.8 km/s, respectively). Despite this large freedom offered to the optimization procedure, most of the radiating points of the middle and end of the rupture are close to the 3 km/s rupture velocity line (shown by the blue dotted line). The brutal moment release, 20–30 s after rupture initiation, of points located 20–50 km from hypocenter clearly appears in this figure.

during the first 20 s of the earthquake (see snapshot at t = 20 s on Figure 2). Then, in the time interval 20–35 s, this area broke almost simultaneously (Figure 3), with maximum slip reaching 12.5 m (Figure 2). Large slip values are mainly distributed near the surface at a depth of 0 to 20 km, which may be the direct cause for the severe destructions in this area.

[11] We carried out some inversion tests to examine the robustness of this delayed and brutal rupture of the main slip patch. We first try to simulate the strong motion records using the constant rupture velocity proposed by other studies [*Wang et al.*, 2008; *Z. Zhang et al.*, 2009; *Xu et al.*, 2009; *Zhang and Ge*, 2010]. However, a systematic increase of the misfit error is observed in all these inversion schemes. Then we conduct an inversion during which the duration for each subfault is reduced from 16 s to 12 s, indicating that the delaying of the rupture is not fully allowed. In this particular inversion, the global rms increases (0.54 compared to 0.42), mostly because the waveform fitting at stations close to the main slip patch is significantly worsened (Figure 4). Figure S7 shows the corresponding fit at all stations and can be compared with the waveform agreement of the optimal model (Figure S6). These inversion tests confirm that the main patch has not simply slipped during the NorthEast propagation of the rupture front. Instead, slippage occurred later, in an almost simultaneous way (Figure 3).

4. Discussions and Conclusions

[12] The rupture process of the Wenchuan earthquake is well determined by the high density of local strong motion data. Our analysis identifies a dominant slip patch located 20–50 km Northeast of the hypocenter, and three other slip areas located further Northeast (at 90 km, 130 km and 190 km respectively), in agreement with the geodetic studies of *Tong et al.* [2010], *Xu and Song* [2010] and *Zhang et al.* [2011]. When looking only at the global behaviour of the rupture kinematics, these patches appear to break during a ~3 km/s Northeast rupture propagation, which is consistent with teleseismic data [*Xu et al.*, 2009; *Zhang et al.*, 2010]. However, while the latter dataset is limited to a general description of the earthquake, local strong motion data are able to describe how rupture has developed inside the main slip areas. In this respect, slippage of the main slip patch is particularly interesting: our study shows that, while this area is located close to the hypocenter, very little slip occurs during the first 20 s after rupture initiation. Then, this 30 km-long patch broke almost simultaneously, with more than 10 m slip released during a 10–15 s time interval.

[13] Such a rupture behavior appears to be typical of the presence of a strong asperity, in the sense first described by *Kanamori and Stewart* [1978]. In this model, seismic slip occurs on strongly stressed areas, where large stress drop facilitates the development of the dynamic rupture. These areas are thought to have a strong resistance to slip, so that their stress has not been released for a long time. During this time of stress build-up, this asperity thus acts as a barrier [*Das and Aki*, 1977]. During the Wenchuan earthquake, rupture development on the main slip patch is fully consistent with the breaking of an asperity. Because of a strong resistance to slip, the initial and moderate stress increase created by slip around the hypocentral region has not been sufficient to trigger the slippage in the asperity. The resistance to slip has been only overcome later, when slip has completely surrounded the asperity, resulting in a stronger stress increase.

[14] Because of the delayed rupture of this asperity, the Wenchuan earthquake can be described as a "compound" rupture. As a matter of fact, seismic slip did not occur only as a consequence of the stress release at the rupture front. Instead, the increase of stress all around the asperity gave birth to a secondary rupture, in which the asperity has

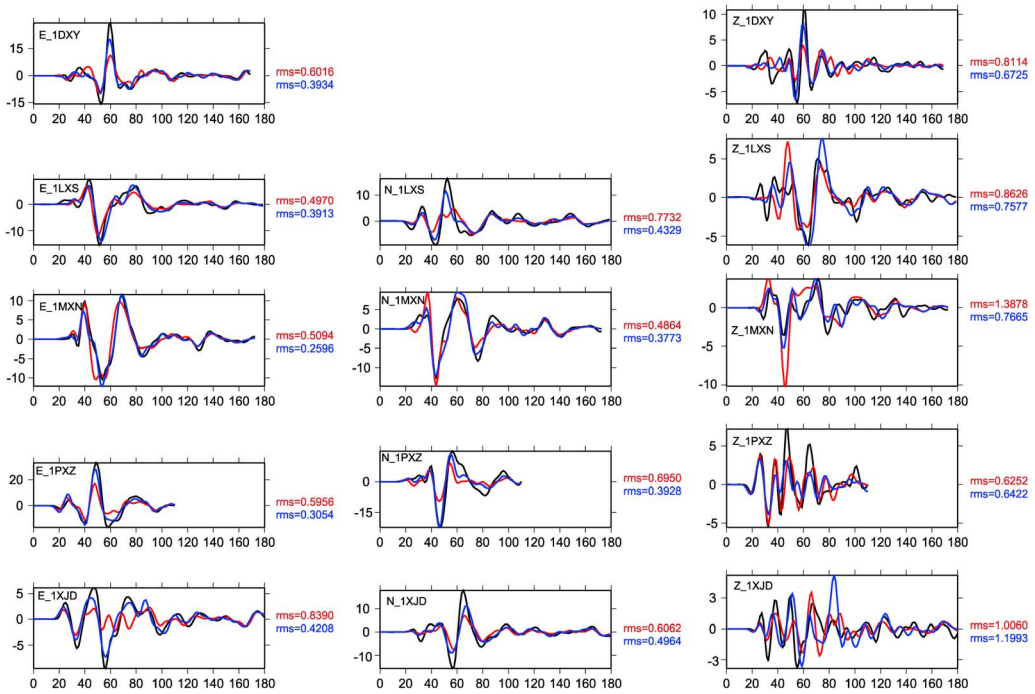

Figure 4. Waveforms agreement for two inversion scenarios. Stations are selected close to and around the main slip patch for comparisons of the inversion test and the optimal inversion. The black lines are the observed waveforms. The blue and red lines are the optimal inversion results and the inversion test results (where rupture delay is not fully allowed), respectively. The rms values of each component from these two inversions are also shown to the right side, marked with the color corresponding to their waveforms. The presented stations are marked with red in Figure 1.

slipped. This compound earthquake behaviour has been previously proposed, in particular for the 2001 Peru earthquake [*Robinson et al.*, 2006; *Lay et al.*, 2010]. In this case, *Lay et al.* [2010] underlined the fact that the compound model is only a realistic scenario, because of the limited resolution of the teleseismic data. The Wenchuan earthquake, where the compound model is strongly supported by the presence of numerous local data, appears to be a better-documented example of this behaviour. It illustrates how the earthquake process may be partitioned between rupture occurring at the rupture front, and secondary triggered ruptures.

[15] **Acknowledgments.** This work is co-supported by grants of Chinese National Science Foundation (41111140386), Basic Scientific Funding of Institute of Geology, China Earthquake Administration (IGCEA1202) and Geoazur laboratory (Nice, France, Internal BQR). The topographic data is downloaded from: http://srtm.csi.cgiar.org. Figures are generated by Generic Mapping Tools [*Wessel and Smith*, 1998].

[16] The Editor thanks Kuvvet Atakan and an anonymous reviewer for assisting in the evaluation of this paper.

References

Alessandrini, B., M. Cattaneo, M. Demartin, M. Gasperini, and V. Lanza (1994), A simple P-wave polarization analysis: Its application to earthquake location, *Ann. Geofis.*, *38*, 883–897.

Bjerrum, L. W., B. Mathilde, M. B. Søørensen, and K. Atakan (2010), Strong Ground-motion simulation of the 12 May 2008 Mw 7.9 Wenchuan earthquake, using various slip models, *Bull. Seismol. Soc. Am.*, *100*, 2396–2424, doi:10.1785/0120090239.

Burchfiel, B. C., et al. (2008), A geological and geophysical context for the Wenchuan earthquake of 12 May 2008, Sichuan, People's Republic of China, *GSA Today*, *18*(7), 4–11, doi:10.1130/GSATG18A.1.

Das, S., and K. Aki (1977), Fault plane with barriers: A versatile earthquake model, *J. Geophys. Res.*, *82*(36), 5658–5670, doi:10.1029/JB082i036p05658.

Delouis, B., D. Giardini, P. Lundgren, and J. Salichon (2002), Joint inversion of InSAR, GPS, teleseismic, and strong-motion data for the spatial and temporal distribution of earthquake slip: Application to the 1999 Izmit Mainshock, *Bull. Seismol. Soc. Am.*, *92*(1), 278–299, doi:10.1785/0120000806.

Feng, G., E. A. Hetland, X. Ding, Z. Li, and L. Zhang (2010), Coseismic fault slip of the 2008 M_w 7.9 Wenchuan earthquake estimated from InSAR and GPS measurements, *Geophys. Res. Lett.*, *37*, L01302, doi:10.1029/2009GL041213.

Guo, Z., K. Deng, and Y. Han (1996), *Formation and Evolution of the Sichuan Basin*, 200 pp., Geol. Publ. House, Beijing.

Ishii, M., P. M. Shearer, H. Houston, and J. E. Vidale (2005), Extent, duration and speed of the 2004 Sumatra-Andaman earthquake imaged by the Hi-Net array, *Nature*, *435*(7044), 933–936, doi:10.1038/nature03675.

Ji, C., and G. Hayes (2008), Preliminary result of the May 12, 2008 Mw 7.9 Eastern Sichuan, China earthquake, report, U.S. Geol. Surv., Reston, Va. [Available at http://earthquake.usgs.gov/eqcenter/eqinthenews/2008/us2008ryan/finite_fault.php.]

Kanamori, H., and G. S. Stewart (1978), Seismological aspects of the Guatemala earthquake of February 4, 1976, *J. Geophys. Res.*, *83*, 3427–3434, doi:10.1029/JB083iB07p03427.

Krüger, F., and M. Ohrnberger (2005), Tracking the rupture of the Mw = 9.3 Sumatra earthquake over 1,150 km at teleseismic distance, *Nature*, *435*, 937–939, doi:10.1038/nature03696.

Lay, T., C. J. Ammon, A. R. Hutko, and H. Kanamori (2010), Effects of kinematic constraints on teleseismic finite-source rupture inversions: Great Peruvian earthquakes of 23 June 2001 and 15 August 2007, *Bull. Seismol. Soc. Am.*, *100*, 969–994, doi:10.1785/0120090274.

Li, X., et al. (2008), Strong motion observations and recordings from the great Wenchuan Earthquake, *Earthquake Eng. Eng. Vib.*, *7*(3), 235–246, doi:10.1007/s11803-008-0892-x.

Meng, Q., E. Wang, and J. Hu (2005), Mesozoic sedimentary evolution of the northwest Sichuan basin: Implication for continued clockwise rotation of the South China block, *Geol. Soc. Am. Bull.*, *117*(3), 396–410, doi:10.1130/B25407.1.

Menke, W. (1985), Imaging fault slip using teleseismic waveforms: Analysis of a typical incomplete tomography problem, *Geophys. J. R. Astron. Soc.*, *81*, 197–204, doi:10.1111/j.1365-246X.1985.tb01358.x.

Olson, A. H., and R. J. Aspel (1982), Finite fault and inverse theory with applications to the 1979 Imperial Valley earthquake, *Bull. Seismol. Soc. Am.*, *72*, 1969–2001.

Robinson, D. P., S. Das, and A. B. Watts (2006), Earthquake rupture stalled by a subducting fracture zone, *Science*, *312*, 1203–1205, doi:10.1126/science.1125771.

Scherbaum, F., and J. Johnson (1990), Pitsa 3.0: A system for doing station based seismological signal processing, paper presented at the 32nd General Assembly of the European Seismological Commission, Eur. Seismol. Comm., Montpellier, France, 6–10 Sept.

Shen, Z. K., et al. (2009), Slip maxima at fault junctions and rupturing of barriers during the 2008 Wenchuan earthquake, *Nat. Geosci.*, *2*, 718–724, doi:10.1038/ngeo636.

Tong, X., D. T. Sandwell, and Y. Fialko (2010), Coseismic slip model of the 2008 Wenchuan earthquake derived from joint inversion of interferometric synthetic aperture radar, GPS, and field data, *J. Geophys. Res.*, *115*, B04314, doi:10.1029/2009JB006625.

Wang, W. M., L. F. Zhao, J. Li, and Z. Yao (2008), Rupture process of the Ms 8.0 Wenchuan earthquake of Sichuan, China, *Chin. J. Geophys.*, *51*(5), 1403–1410.

Wen, Z., J. Xie, M. Gao, Y. Hu, and K. T. Chau (2010), Near-source strong ground motion characteristics of the 2008 Wenchuan earthquake, *Bull. Seismol. Soc. Am.*, *100*(5B), 2425–2439, doi:10.1785/0120090266.

Wessel, P., and W. H. F. Smith (1998), New, improved version of Generic Mapping Tools released, *Eos Trans. AGU*, *79*(47), 579, doi:10.1029/98EO00426.

Xu, Z. J., and X. Song (2010), Joint inversion for crustal and Pn velocities and Moho depth in Eastern Margin of the Tibetan Plateau, *Tectonophysics*, *491*(1–4), 185–193, doi:10.1016/j.tecto.2009.11.022.

Xu, Y., K. D. Koper, O. Sufri, L. Zhu, and A. R. Hutko (2009), Rupture imaging of theMw7.9 12 May 2008 Wenchuan earthquake from back projection of teleseismic P waves, *Geochem. Geophys. Geosyst.*, *10*, Q04006, doi:10.1029/2008GC002335.

Zhang, H., and Z. Ge (2010), Tracking the rupture of the 2008 Wenchuan earthquake by using the relative back-projection method, *Bull. Seismol. Soc. Am.*, *100*, 2551–2560, doi:10.1785/0120090243.

Zhang, Y., et al. (2009), Spatio-temporal rupture process of the 2008 great Wenchuan earthquake, *Sci. China Ser. D*, *52*(2), 145–154, doi:10.1007/s11430-008-0148-7.

Zhang, Z., Y. Wang, Y. Chen, G. A. Houseman, X. Tian, E. Wang, and J. Teng (2009), Crustal structure across Longmenshan fault belt from passive source seismic profiling, *Geophys. Res. Lett.*, *36*, L17310, doi:10.1029/2009GL039580.

Zhang, P. Z., et al. (2010), Oblique, High-Angle, Listric-Reverse Faulting and Associated Development of Strain: The Wenchuan Earthquake of May 12, 2008, Sichuan, China, *Annu. Rev. Earth Planet. Sci.*, *38*, 353–382, doi:10.1146/annurev-earth-040809-152602.

Zhang, G. H., et al. (2011), Slip distribution of the 2008 Wenchuan Ms 7.9 earthquake by joint inversion from GPS and InSAR measurements: A resolution test study, *Geophys. J. Int.*, *186*, 207–220, doi:10.1111/j.1365-246X.2011.05039.x.